AIAA JOURNAL
Vol. 48, No. 10, October 2010

Influence of Hall Effect on Electrodynamic Heat Shield System for Reentry Vehicles

Hirotaka Otsu*
Shizuoka University, Shizuoka 432-8561, Japan
Detlev Konigorski†
EADS Astrium, Bremen 28199, Germany
and
Takashi Abe‡
Japan Aerospace Exploration Agency (JAXA), Kanagawa 229-8510, Japan

DOI: 10.2514/1.40372

The influence of the Hall effect on the magnetic flow control to a reentry vehicle with a hemispherical nose and the imposed dipole magnetic field was investigated. For this purpose, a parametric study for the Hall parameter was conducted. The present result shows that the Hall effect drastically affects the electric potential distribution and electric current pattern inside the shock layer, depending on the vehicle surface conductivity, but it does not affect the current strength in the circumferential direction in the case of the insulating wall. As a result, the shock-standoff distance does not change, even if the Hall effect is significant when the vehicle surface is regarded as an insulating wall. The present parametric study clarified that this conclusion is applicable in a wide variety of the Hall parameter and enables us to get an insight of the mechanism behind the phenomenon. This conclusion suggests that, if the vehicle surface is regarded as an insulating wall, the magnetic flow control for the reentry vehicle will prove to still be a useful technology, even when the Hall effect is taken into account.

Nomenclature

$\mathbf{B}$	=	magnetic field vector
B	=	magnetic field strength $\lvert\mathbf{B}\rvert$
$\mathbf{b}$	=	unit vector defined by $\mathbf{B}/B$
C_H	=	Hall parameter
$\mathbf{E}$	=	electric field vector $(E_r, 0, E_z)$
e	=	elementary charge
J	=	electric current density, $\mathrm{A/m^2}$
$\mathbf{J}$	=	electric current density vector (J_r, J_θ, J_z)
N_e	=	number density of free electron, $1/\mathrm{m^3}$
$\mathbf{V}$	=	velocity vector (u_r, u_θ, u_z)
σ	=	electric conductivity, $\mathrm{S/m}$
ϕ	=	electric potential, V

I. Introduction

FOR typical thermal protection systems (TPS) applied to reentry vehicles, various materials that can withstand the severe aerodynamic heating are employed. A typical TPS is easily damaged, since it is exposed to a severe reentry heating; thus, it needs to be replaced or refurbished for the next flight. This indicates that a typical TPS is not suitable for a future reusable space transportation system. As one candidate of the alternatives of a typical TPS, a heat shield system that uses the electrodynamic force has attracted much attention recently. Such a system is called the electrodynamic heat shield system (EDH). In this system, the strong magnetic field is generated around the reentry vehicle, which produces the Lorentz force acting on the flow through an interaction with the ionized flow behind the strong bow shock. The Lorentz force thus produced is used to control the flow around the reentry vehicle, as illustrated in Fig. 1, so that, for instance, the heat flux is reduced. In this figure, $\mathbf{J}$, $\mathbf{B}$, and $\mathbf{V}$ are the electric current vector, magnetic field vector, and flow velocity vector, respectively. The dashed line shows the bow shock affected by the applied Lorentz force $\mathbf{J} \times \mathbf{B}$. Also in this figure, the vehicle geometry is assumed to be a cylinder with a hemispherical nose, and the magnetic dipole is assumed at the center of the sphere. The situation represented in Fig. 1 is more or less realizable when the Hall effect can be assumed to be negligible. In fact, under this assumption, the analytical and numerical verification of the magnetic flow control for the reentry vehicle was clearly demonstrated [1]. In the case of typical orbital or suborbital reentry flight conditions, however, the Hall effect is expected to be strong [2]. When the Hall effect is strong, the Hall current may create the electric field, which does not appear under the condition that the Hall effect is negligible. Such an induced electric field may affect the electric current and, subsequently, modify the Lorentz force and the efficiency of EDH.

Although most of the previous research does not take account of the Hall effect, the impact of the Hall effect was investigated analytically and numerically by some researchers [3–5]. Levy [3] analytically investigated the two-dimensional plasma flow around a cylinder with an imposed magnetic field, which is created by the current in the wire parallel to the axis of the cylinder. In this research, he concluded that the interaction between the magnetic field and the plasma flow was weakened because the current strength around the cylinder was reduced by the Hall effect. Porter and Cambel [4] investigated the plasma flow around a sphere with the imposed magnetic field. In this study, however, they simplified the governing equations to analytically calculate the flowfield around the stagnation region. As a result, they also showed that the Hall effect weakens the efficiency of this system. Recently, Fujino et al. [5,6] have performed computational fluid dynamics (CFD) analyses for a magnetic flow control for a reentry vehicle including the Hall effect. In their study, they investigated a three-dimensional flow around an axis-symmetry body and solved a full Navier–Stokes equation, including the non-equilibrium chemical reactions. In contrast to the previous studies, they showed that the Hall effect does not affect the efficiency of EDH when the vehicle surface is regarded as an insulating wall. In their

Presented as Paper 2005-5049 at the 36th AIAA Plasmadynamics and Lasers Conference, Toronto, ON Canada, 6–9 June 2005; received 13 August 2008; revision received 17 May 2010; accepted for publication 17 May 2010.

*Associate Professor, Department of Mechanical Engineering, 3-5-1 Johoku, Naka-ku, Hamamatsu; currently Associate Professor, Department of Mechanical and Systems Engineering, Ryukoku University. Senior Member AIAA.

†Technical Engineer, Huenefeldstrasse 1-5. Member AIAA.

‡Professor, Institute of Space and Astronautical Science, 3-1-1 Yoshinodai, Sagamihara. Associate Fellow AIAA.

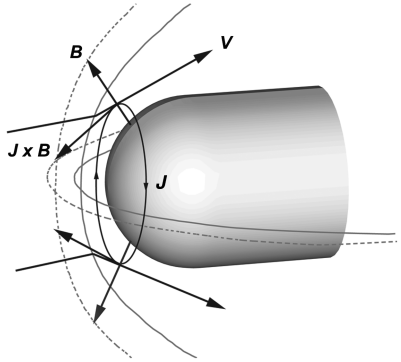

Fig. 1 Schematic view of the plasma flow around the vehicle with the applied magnetic field and the Lorentz force.

simulation, the Hall parameter was self-consistently determined through the chemical reaction model implemented in their nonequilibrium flow simulation code. Since the Hall parameter, thus determined, appears simultaneously with the EDH, the Hall effect appears on the flow in a manner combined with the EDH. Therefore, the mechanism of how the Hall effect appears was not clarified. In such a way, to adequately evaluate how the Hall effect affects the efficiency of EDH, their simulation, even though the simulation may include the nonequilibrium chemical effect, is not sufficient. Furthermore, their method is not sufficient to get a precise prediction of the EDH affected by the Hall effect for a specific flight condition, since it is widely acknowledged that the current chemical reaction model cannot avoid uncertainty for a prediction of the ionization rate or the Hall parameter. In other words, the Hall parameter, thus determined by the simulation, cannot avoid uncertainty; therefore, the simulation result cannot avoid inherent uncertainty in the Hall effect. To evaluate the influence of the uncertainty in the Hall effect, it is necessary to understand how the Hall effect appears parametrically. This understanding may enable us to understand the mechanism of the Hall effect. This understanding is also quite helpful to evaluate how the Hall effect appears during the reentry flight in which the Hall parameter varies widely.

In the present study, we clarify the influence of the Hall effect on the magnetic flow control and estimate the efficiency of EDH. Furthermore, we will clarify the mechanism of how such an influence of the Hall effect appears. For this purpose, we conducted a simplified CFD analysis, taking account of the Hall parameter as a parameter.

II. Governing Equations and Physical Models

We consider an axisymmetric three-dimensional flow around a sphere, with the magnetic field created by a dipole mounted inside a sphere. The magnetic field is defined by the magnetic dipole

$$\mathbf{B} = \frac{\mu_0}{4\pi}\left[\frac{3\mathbf{r}(\mathbf{r}\cdot\mathbf{m}) - r^2\mathbf{m}}{r^5}\right] \tag{1}$$

where μ_0 and $\mathbf{r}$ are the magnetic permeability of the vacuum and the positional vector measured from the magnetic dipole, respectively. Here, $\mathbf{m}$ is a vector parallel to the axis of symmetry, and $|\mathbf{m}|$ reflects the strength of the magnetic dipole. The axis of the dipole is parallel to the vehicle axis, as illustrated in Fig. 1.

In a typical reentry condition, a strong shock wave is formulated in front of the vehicle, and a weakly ionized flow is generated in the shock layer formulated between the vehicle surface on the shock front, since the temperature in the shock layer is very much elevated. Such a weakly ionized flow is generated through the chemical reaction, including the ionization, of the atmosphere caused by the elevated temperature originating from the shock compression. When the magnetic field is applied to such a weakly ionized flow, we can expect that the effect of EDH appears, as Poggie and Gaitonde demonstrated, based on the simplified flow simulation [1]. In reality, however, the behavior of the interaction becomes very complicated (since the interaction depends on the local plasma characteristics, which are determined self-consistently with chemically reacting flow dynamics and the imposed magnetic field) and varies from place to place. Therefore, it is suitable to employ a simple flow model to get an insight on the mechanism of the interaction and the Hall effect. Thus, in the present study, we did not take account of real gas effects, such as chemical reactions and thermochemical nonequilibrium effects, but we assumed an ideal gas with electrical conduction. To investigate the flowfield and the electric and magnetic field simultaneously, we need to solve the Navier–Stokes equations and the Maxwell equations. When the magnetic Reynolds number is small enough, the induced magnetic field is very weak and negligible when compared with the imposed magnetic field. Thus, we do not need to solve the Maxwell equations. This assumption is called the low-magnetic Reynolds number assumption [1].

Under this assumption, in order to take account of the electromagnetic effect, we need to add the terms related to the electromagnetic force and the joule heating to Navier–Stokes equations as magnetic source terms. In the present study, the body configuration and the applied magnetic field are assumed to be axisymmetric. Under these assumptions, the governing equations can be expressed in the following form:

$$\frac{\partial \mathbf{U}}{\partial t} + \frac{\partial \mathbf{F}}{\partial r} + \frac{\partial \mathbf{G}}{\partial z} + \frac{1}{r}\mathbf{S}_r = \mathbf{S}_M \tag{2}$$

$$\mathbf{U} = (\rho, \rho u_r, \rho u_\theta, \rho u_z, \rho E_t)^T \tag{3}$$

$$\mathbf{S}_M = (0, \mathbf{J}\times\mathbf{B}, \mathbf{J}\cdot\mathbf{E})^T \tag{4}$$

where $\mathbf{F}$ and $\mathbf{G}$ are flux vectors including viscous terms, and $\mathbf{S}_r$ and $\mathbf{S}_M$ are the source term vector related to the axisymmetric flow and the source term vector related to the Lorentz force and the joule heating, respectively. E_t, ρ, $\mathbf{J}$, and $\mathbf{E}$ are total energy, density, electric current density, and electric field, respectively.

The electric current density $\mathbf{J}$ can be described as

$$\mathbf{J} = \sigma(\mathbf{E} + \mathbf{V}\times\mathbf{B}) - C_H(\mathbf{J}\times\mathbf{b}) \tag{5}$$

where C_H is Hall parameter defined by

$$C_H = \frac{\sigma B}{N_e e} \tag{6}$$

and $\mathbf{b}$ is a unit vector defined as follows:

$$\mathbf{b} = \mathbf{B}/B = (b_r, 0, b_z)^T \tag{7}$$

Equation (5) can be rewritten in the following tensorial form:

$$\mathbf{J} = \tilde{\sigma}(\mathbf{E} + \mathbf{V}\times\mathbf{B}) \tag{8}$$

where $\tilde{\sigma}$ is a tensor and defined by

$$\tilde{\sigma} = \frac{\sigma}{1+C_H^2}\begin{bmatrix} 1+C_H^2 b_r^2 & -C_H b_z & C_H^2 b_r b_z \\ C_H b_z & 1 & -C_H b_r \\ C_H^2 b_r b_z & C_H b_r & 1+C_H^2 b_z^2 \end{bmatrix} \tag{9}$$

The electric current density is governed by the electric current continuity condition:

$$\nabla\cdot\mathbf{J} = 0 \tag{10}$$

Even though we assume a simple gas model with certain electrical conduction, the electric number density and/or the electric conductivity are cautiously taken into account. First of all, the electric conductivity and the Hall parameter are set to be negligibly small (or $1.0\mathrm{e}-5$) outside of the shock layer, so that their effect can be neglected. The boundary of the shock layer is determined by a temperature jump. The region where the temperature is higher than twice the ambient temperature T_∞ is defined to be inside the shock

layer. Second, we assume that they vary inside the shock layer, depending on the flow properties, since they have a direct influence on the magnetic flow control. In this study, we assumed that the electric conductivity and the electron number density are dependent on the temperature; that is,

$$\sigma = \sigma_r \left(\frac{T}{T_r}\right)^2, \qquad N_e = N_{e,r}\left(\frac{T}{T_r}\right)^2 \tag{11}$$

where σ_r and $N_{e,r}$ are reference values, and T_r is a reference temperature defined as the highest temperature inside the shock layer. This relationship is used to take account of the temperature dependency on both the electric conductivity and the electron number density. A similar relationship for the electric conductivity is employed in [1]. Then, the Hall parameter can be rewritten as

$$C_H = \frac{\sigma B}{N_e e} = \frac{\sigma_r B}{N_{e,r} e} \tag{12}$$

For the numerical computations, the governing equations were rewritten in nondimensional form. The equations are nondimensionalized by the reference quantities ρ_r, V_r, L_r, B_r, T_r, and σ_r. The nondimensional variables are then

$$t^* = tV_r/L_r, \quad \rho^* = \rho/\rho_r, \quad \mathbf{V}^* = \mathbf{V}/V_r, \quad \mathbf{B}^* = \mathbf{B}/B_r$$
$$p^* = p/\rho_r V_r^2, \quad E_t^* = E_t/V_r^2, \quad \sigma^* = \sigma/\sigma_r$$
$$J^* = J/\sigma_r V_r B_r, \quad T^* = T/T_r \tag{13}$$

In the present study, the reference values for the magnetic field and the electrical conductivity were taken to be those at the stagnation point. The reference length scale was the body radius, and the other reference values corresponded to the freestream conditions. In the subsequent discussion, the superscript (*) will be dropped, and all quantities will be assumed to be nondimensional unless explicitly stated otherwise. The overall form of the governing equation is unchanged by nondimensionalization. The magnetic source terms become

$$\mathbf{J} \times \mathbf{B} = Q[\sigma(\mathbf{E} + \mathbf{V} \times \mathbf{B}) \times \mathbf{B} - C_H(\mathbf{J} \times \mathbf{b}) \times \mathbf{B}] \tag{14}$$

$$\mathbf{J} \cdot \mathbf{E} = Q[\sigma(\mathbf{E} + \mathbf{V} \times \mathbf{B}) \cdot \mathbf{E} - C_H(\mathbf{J} \times \mathbf{b}) \cdot \mathbf{E}] \tag{15}$$

where $Q = \sigma_r B_r^2 L_r/(\rho_r V_r)$ is the magnetic interaction parameter. The Hall parameter can be rewritten as

$$C_H = C_{H,r}|\mathbf{B}^*| \tag{16}$$

where

$$C_{H,r} = \frac{\sigma_r B_r}{N_{e,r} e} \tag{17}$$

As can be seen from the magnetic source terms (14) and (15), the flowfield is governed by the two nondimensional parameters Q and $C_{H,r}$, which are determined simultaneously for a specific flow condition and the magnetic field strength but cannot be determined independently. However, Poggie and Gaitonde [1] succeeded in demonstrating the effect of Q, intentionally neglecting the effect of $C_{H,r}$. That is, they demonstrated that the electrodynamic shield effect appears as a result of Q. In contrast, Fujino et al. [5,6] recently showed that the electrodynamic shield effect is strongly affected by the effect of $C_{H,r}$ by their simulation, which includes the nonequilibrium chemical reaction effect. Nevertheless, it was still unclear how the effect of $C_{H,r}$ appears, since both the parameters are determined self-consistently in their simulation; hence, the phenomenon remains complicated. Therefore, after the strategy taken by Poggie and Gaitonde [1] to demonstrate how the effect of Q appears to be neglecting the effect of $C_{H,r}$ intentionally, we will vary $C_{H,r}$ intentionally in the present study, which will enable us to understand how the effect of $C_{H,r}$ appears. That is, we will carry out a parametric study for $C_{H,r}$.

III. Numerical Method and Boundary Conditions

The governing equations are discretized by using the finite-volume method. The numerical flux is evaluated by the advection upstream splitting method (AUSM)-DV scheme [7], where DV denotes the convective part of the momentum flux of the AUSM-DV scheme consisting of the blending of the flux-difference and flux-vector procedures. The time integration is performed using the matrix-free Gauss–Seidel method [8]. The point-implicit method is also used to treat the source term related to electromagnetic effects implicitly.

The electric current continuity condition [Eq. (10)] is solved in the following way. For this purpose, the electric potential ϕ is introduced;

$$\mathbf{E} = -\nabla\phi \tag{18}$$

Then, the equation to be solved becomes

$$\nabla \cdot \tilde{\sigma}(-\nabla\phi + \mathbf{V} \times \mathbf{B}) = 0 \tag{19}$$

This is a Poisson equation for electric potential ϕ. This equation should be solved at each time step with Eq. (2). Nevertheless, since we need a steady-state solution, the variation of ϕ in time is not expected to be important. Thus, the above equation is solved every 1000 time steps. Equation (19) is numerically solved in an iterative manner, in which 200 iterations are necessary to reduce the residual of the electric potential ϕ of up to $1.0e-4$ at each time step. To obtain a converged solution for other flow properties, 200,000 time steps for solving Eqs. (2) and (19) were needed.

The computational grid is created around the sphere with a radius of 1.0 m, as shown in Fig. 2. This computational grid has 31 points along the surface and 50 points along the line normal to the body surface.

As a boundary condition on the surface, the temperature is assumed to be constant. The surface pressure is determined by the following relationship:

$$\frac{\partial p}{\partial \eta} = 0 \tag{20}$$

where η is the direction normal to the body surface.

The boundary condition for the electric potential is as follows. The electric potential at the far boundary (boundary C–D) is set to be 0 V, and on the axis of symmetry (boundary D–A) and the outflow boundary (boundary B–C), the potential is determined by the following relationship:

$$\mathbf{J} \cdot \mathbf{n} = 0 \tag{21}$$

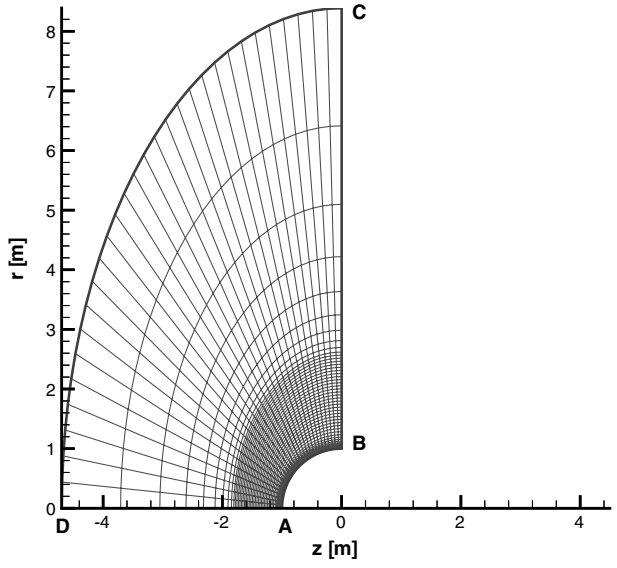

Fig. 2 Computational grid around the sphere.

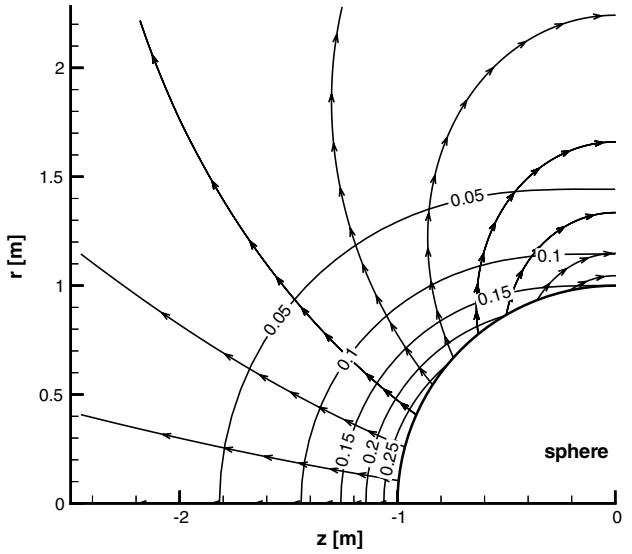

Fig. 3 Magnetic field distribution around the sphere.

where **n** is the unit vector normal to each boundary. This condition means that the electric current flows along the boundary. The validity of this boundary condition on the boundary B–C is discussed in the following section.

As for the body surface conductivity, we assume two different conditions: conducting wall and insulating wall. In the case of the conducting wall condition, the electric potential ϕ should be constant along the body surface. The absolute value of the electric potential, however, is not obvious. Takizawa et al. [9] experimentally investigated the effect of the surface electric potential value on the plasma flow around a conducting body. Their results showed that the effect of the electric potential has no significant impact on the flowfield around a conducting body, such as the shock layer thickness and the temperature distribution. Thus, in the present study, the electric potential ϕ on the surface (boundary A–B) is set to be 0 V and, in the case of the insulating wall condition, the electric potential ϕ is calculated by imposing the following condition:

$$\mathbf{J} \cdot \mathbf{n} = 0 \tag{22}$$

IV. Results and Discussions

As a typical flight condition, we assume that the reentry velocity is 6500 m/s at an altitude of 69 km. The surface temperature is assumed to be 2000 K. The body geometry is a sphere with a radius of 1.0 m. The magnetic field is created by the magnetic dipole located at the center of the sphere. The magnetic field lines and strength are shown in Fig. 3. Based on the flowfield calculation for the body without the magnetic field, the typical plasma characteristics for the typical flight condition were assessed. The flowfield calculation includes an effect of nonequilibrium chemical reactions. Based on

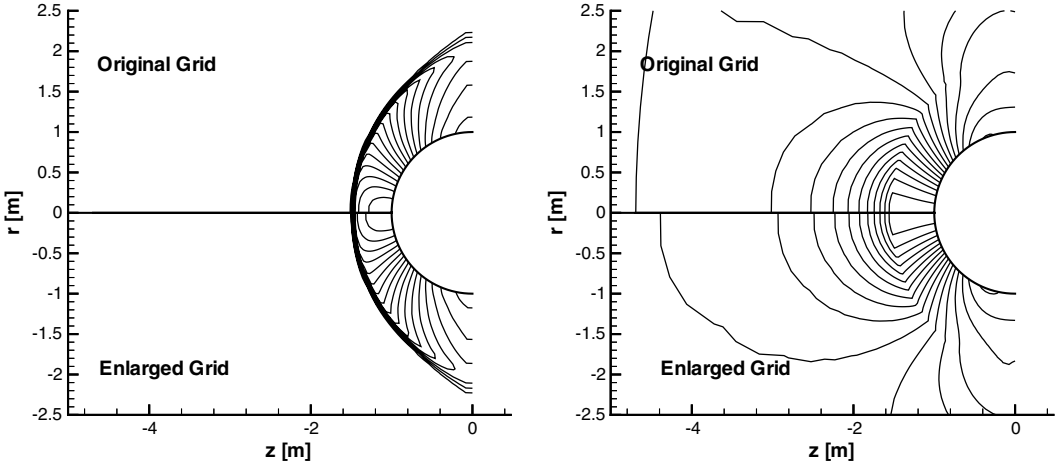

a) Pressure **b) Electric potential**

Fig. 4 Effect of the dimension of the computational domain on the flowfield.

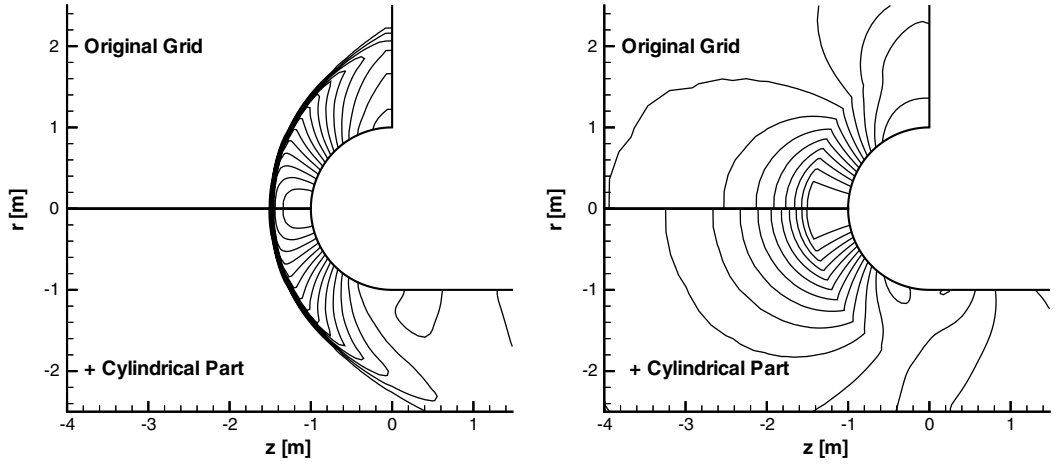

a) Pressure **b) Electric potential**

Fig. 5 Effect of the location of the boundary B–C on the flowfield.

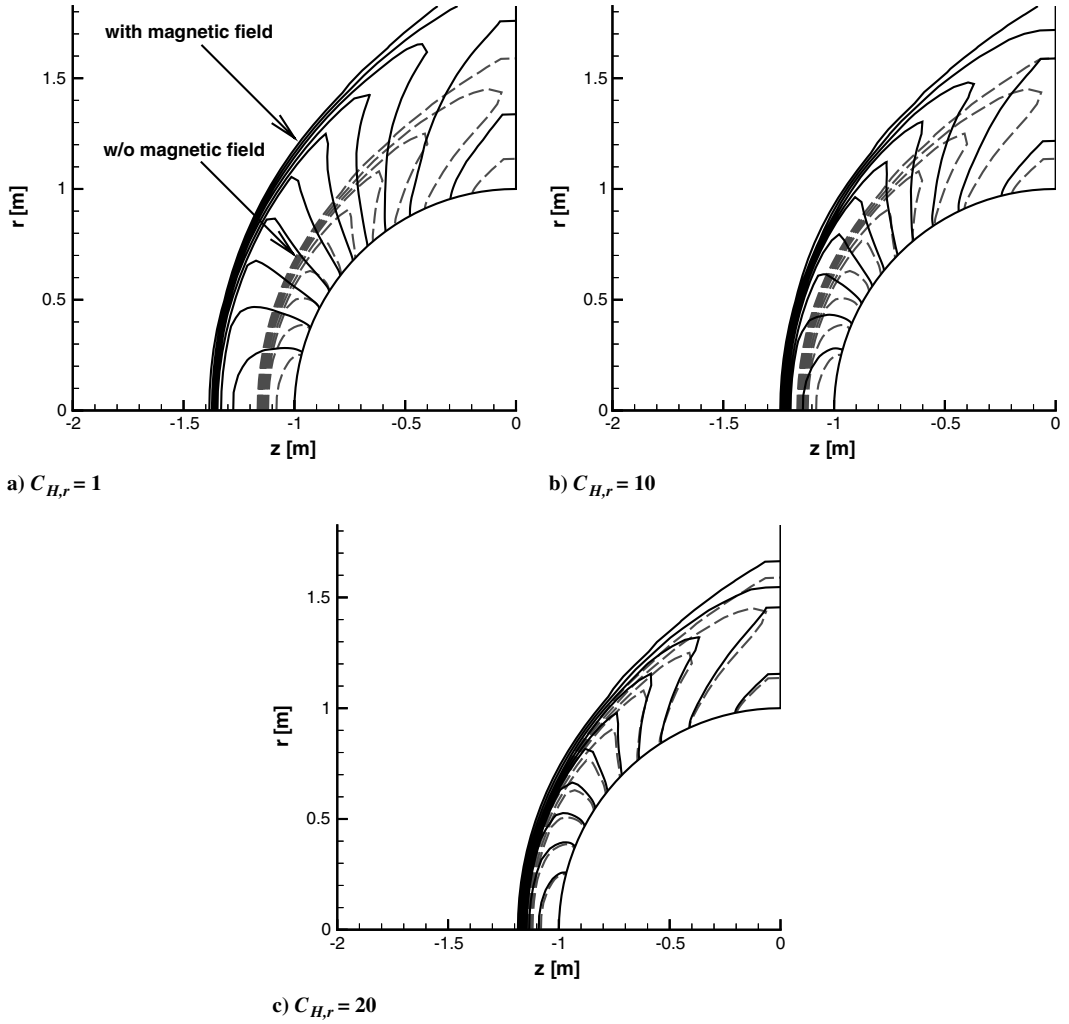

Fig. 6 Effect of the Hall parameter on the pressure distribution with the conducting wall.

the assessment, the electric conductivity σ_r is set to be 200 S/m, and $T_{\max}$ is set to be 25,000 K. The other reference values B_r, $N_{e,r}$, L_r, ρ_r, and V_r are 0.3 T, $1.0\text{e}-19$ $1/\text{m}^3$, 1.0 m, $1.0\text{e}-4$ kg/m^3, and 6500 m/s, respectively. For those reference values, Q and $C_{H,r}$ are calculated as 27.69 and 37.5, respectively. As mentioned before, we aim to investigate the influence of the Hall effect on the flowfield and on the efficiency of the electrodynamic heat shield. Therefore, the parameter of the Hall effect $C_{H,r}$ is intentionally varied, which enables us to investigate how the Hall effect appears on the flowfield.

A. Effect of Computational Domain

In the present study, the distribution of the electric potential ϕ plays a key role since it is directly generated by the Hall effect. In fact, the Hall current in a r-z plane is expected to create the electric potential distribution in the plane, which will affect the entire electric current, Lorentz force, and efficiency of the EDH. The electric potential is determined by the Poisson equation for ϕ, as shown in Eq. (19). In general, the solution of the Poisson equation is sensitive to the treatment of the boundary condition. Therefore, it is necessary to investigate the effect of the outer boundary of the computational domain.

At first, we investigated the effect of the dimension of the computational domain on the flowfield by comparing the solutions for the original and the larger computational domain. As for the boundary condition of the body surface conductivity, we employed the insulating wall condition. Figure 4 shows the distribution of the electric potential and the static pressure around the sphere. $C_{H,r}$ is set to be 20 $1/\text{T}$, and the magnetic field strength at the stagnation point is 0.3 T. The result presented in a domain for $r \geq 0$ is obtained by the original computational grid, and the result in a domain for $r \leq 0$ is obtained by the enlarged computational grid. Points C and D for the original computational grid are located at (0, 8.4 m) and (−4.8 m, 0), respectively, and points C and D for the enlarged computational grid are located at (0, 345 m) and (−175 m, 0), respectively. As seen from Figs. 4a and 4b, we could not find a significant difference between the two results. Thus, we can conclude that the computational domain of the original computational grid shown in Fig. 2 has a sufficient dimension for our present purpose.

Next, we investigated the treatment of the boundary condition on the boundary B–C. On the boundary B–C, we imposed the boundary condition defined by Eq. (21). This condition is only an artificial one, but it is employed here since its adverse effect may not appear significantly in the region around the stagnation point, which is our main concern in this study. Ideally, in order to remove the ambiguity about the treatment of the boundary condition on the boundary B–C, the flowfield including the wake region should be solved. But solving the flowfield including the wake region is very difficult, since the density is very low in the wake region, which may cause the numerical divergence in the calculation. Instead, in this study, we consider an additional cylindrical part added to the sphere, so that the boundary B–C becomes separate from stagnation region, and investigate the influence of the location of the boundary B–C. Figure 5 shows the distribution of the pressure and the electric potential around the body. In the case of the computational domain including the cylindrical part, the boundary B–C is located at $z = 3$ m. As seen from Fig. 5, the difference of the pressure distribution and the electric potential distribution around the sphere appears to be negligible. This is because the current strength is not so strong near the boundary B–C. Additionally, we modified the length

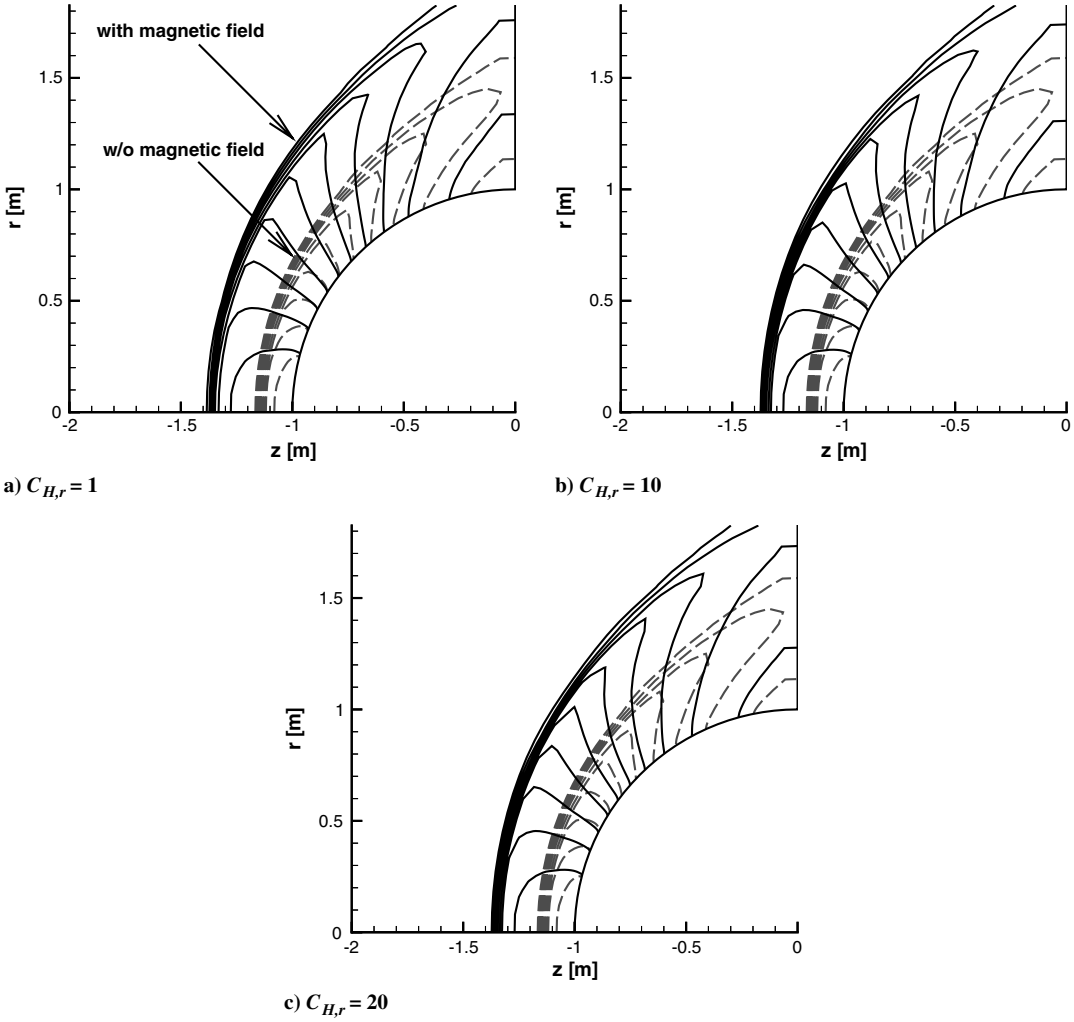

Fig. 7 Effect of the Hall parameter on the pressure distribution with the insulating wall.

of the cylindrical part to investigate the effect of the location of the boundary B–C. The location of the boundary B–C is varied from $z = 1$ m to $z = 10$ m. In all the cases, we could not find any significant influence of the location of the boundary B–C on the distribution of the pressure and the electric potential near the stagnation region. Thus, we can conclude that the location of the boundary B–C in the case of the original grid is reasonable.

B. Impact of Hall Effect on Flowfield

Now, we evaluate the influence of the Hall effect on the flowfield. For this purpose, the Hall parameter $C_{H,r}$ is varied in a wide range including a nominal value. First, we will examine the pressure distribution in the flowfield and the shock-standoff distance around the sphere. Figures 6 and 7 show the pressure contours for the flow around the sphere with the conducting wall and the insulating wall, respectively. In Figs. 6 and 7, the pressure contours without the applied magnetic field (dashed line) are superimposed for comparison. As shown in Fig. 6, we can observe that the shock-standoff distance decreases as the Hall parameter increases. This indicates that the Hall effect weakens the Lorentz force inside the shock layer when the surface is the conducting wall. In contrast to the results with the conducting wall, however, the shock-standoff distance does not change very much, even if the Hall parameter increases, as shown in Fig. 7. This indicates that the Hall effect does not affect the Lorentz force very much when the surface is the insulating wall. The similar trend for the flowfield, for the insulating wall and the conducting wall, is found in [5,6]. However, the present study has clarified that the conclusion is not influenced very much over a wide range of the Hall parameter. During the entire reentry flight trajectory, the Hall parameter varied in a wide range. Hence, we can conclude that the Hall effect will not weaken the efficiency of EDH over the entire reentry flight trajectory. To make this conclusion more definite, however, it is necessary to investigate the details of the Hall effect and to clarify the reason why this phenomenon appears.

As indicated in Eqs. (2–4), the pressure distribution is affected by the Lorentz force $\mathbf{F}_L$:

$$\mathbf{F}_L = \mathbf{J} \times \mathbf{B} \tag{23}$$

Since $\mathbf{B}$, in the present situation, is restricted only in the r-z plane,

$$\mathbf{B} = (B_r, 0, B_z)^T \tag{24}$$

J_r and J_z generate the Lorentz force in a circumferential direction that produces the fluid flow in the circumferential direction. On the contrary, J_θ creates the Lorentz force in the r-z plane, which affects the fluid flow in the r-z plane. Therefore, we can expect that only J_θ is effective in affecting the pressure distribution and the shock-standoff distance. In fact, as shown in Fig. 8, which depicts the distribution of J_θ around the sphere for the insulating and the conducting wall, we can see that the intensity and the distribution of J_θ are quite different between the two cases. Here, $C_{H,r}$ is set to be 20 for the two cases. When the surface is regarded as an insulating wall, the maximum value of J_θ is about $20,000$ A/m^2. In contrast, the maximum value of J_θ for the conducting wall is about 6000 A/m^2, which is much smaller than that for the insulating wall. We can expect that the difference of J_θ leads to the difference of the Lorentz force and the shock-standoff distance, as shown in Figs. 6 and 7, and that J_θ is a very important factor for the EDH.

Now we will investigate the behavior of J_θ affected by the Hall effect. First, it is useful to see the expression of J_θ rewritten by using Eqs. (8) and (9):

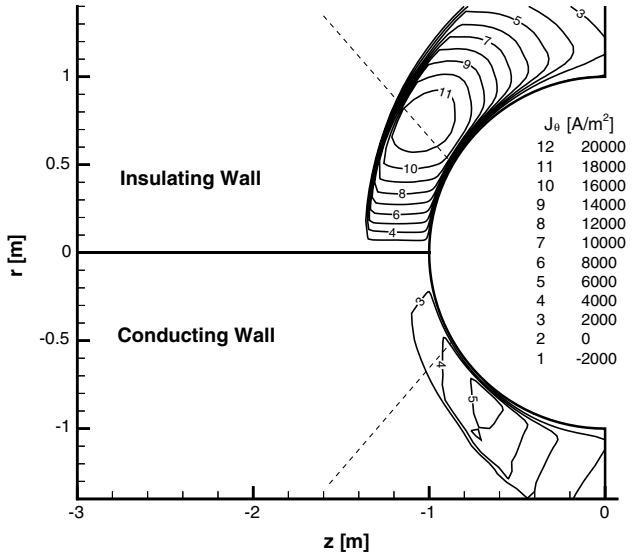

Fig. 8 Distribution of the current in the circumferential direction around the sphere.

$$J_\theta = \frac{\sigma}{1+C_H^2}[-C_H(E_z b_r - E_r b_z) + (u_z B_r - u_r B_z) + C_H u_\theta B]$$
$$= \frac{\sigma}{1+C_H^2}[-C_H(\mathbf{E}\times\mathbf{b})_\theta + (\mathbf{V}\times\mathbf{B})_\theta + C_H u_\theta B] \quad (25)$$

For the Hall parameter, C_H much larger than one, the first term and the third term of the right-hand side of Eq. (25) are proportional to $1/C_H$, and the second term is proportional to $1/C_H^2$. That is, the first term and the third term can be dominant in J_θ when the Hall effect will be significant. Keeping in mind this general behavior of the J_θ against the Hall effect, let us investigate the behavior of J_θ in the simulation result. Figures 9a–9d show the distribution of J_θ along the dashed line indicated in Fig. 8 for the case of the insulating wall with various $C_{H,r}$ varying from 1 to 50 1/T. At first, we can see that the total strength of J_θ is not affected very much, even if $C_{H,r}$ changes widely. This is the reason why the shock-standoff distance does not change so much, as shown in Fig. 7, when the surface is regarded as an insulating wall. Nevertheless, we must note that the strength of each of the three terms in Eq. (25) changes drastically as $C_{H,r}$ changes, as suggested in Eq. (25). Among the three terms in Eq. (25), the main contribution to J_θ is the $\mathbf{V}\times\mathbf{B}$ term for $C_{H,r}$, of 1.0 which corresponds to the case that the Hall effect is negligible. As $C_{H,r}$ increases, the contribution of the $\mathbf{V}\times\mathbf{B}$ term decreases, and the contribution of the $\mathbf{E}\times\mathbf{b}$ term increases. This indicates that, as the Hall effect becomes more significant, the electric field becomes stronger and, as a result, the $\mathbf{E}\times\mathbf{b}$ term becomes dominant in J_θ, which is comparable to the one for the case that the Hall effect is negligible. That is, the main contribution to J_θ changes from the $\mathbf{V}\times\mathbf{B}$ term to the $\mathbf{E}\times\mathbf{b}$ term as the Hall effect becomes significant, and J_θ can be approximated by the $\mathbf{E}\times\mathbf{b}$ term when $C_{H,r}$ is much larger than 20. This means that the main contribution to J_θ changes almost completely from the $\mathbf{V}\times\mathbf{B}$ term to the $\mathbf{E}\times\mathbf{b}$ term within the range of $C_{H,r}$ tested in the present study. This is the key finding in the present study that explains how the Hall effect affects the current

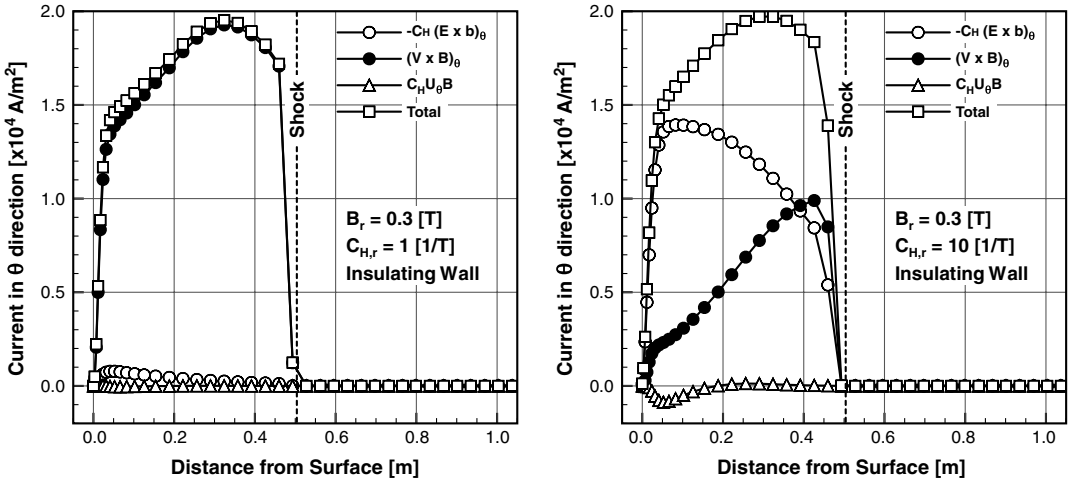

a) $C_{H,r} = 1$

b) $C_{H,r} = 10$

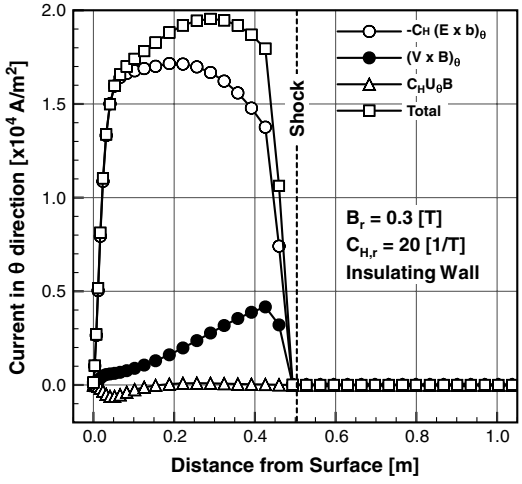

c) $C_{H,r} = 20$

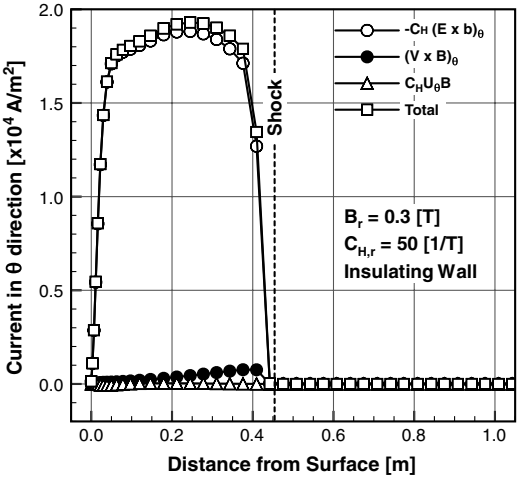

d) $C_{H,r} = 50$

Fig. 9 Effect of the Hall parameter on the current strength in the circumferential direction for the insulating wall.

strength in the circumferential direction J_θ in the case of an insulating wall, and this explanation is well supported by the numerical results in both Fig. 9 and Eq. (25), the mathematical expression of J_θ. And the range of $C_{H,r}$ is large enough to understand the main behavior in the flowfield by the Hall effect. In the real reentry flight condition from low Earth orbit, $C_{H,r}$ may vary from 10 to 1000 1/T. Thus, during most of the reentry flight trajectory, the flowfield will be similar to the one for the case of a $C_{H,r}$ of 50. As compared with other terms, the contribution of the $u_\theta B$ term remains small for all the cases.

The situation for the case with a conducting wall is quite different from that for the case with an insulating wall. That is, as shown in Fig. 10, which depicts the contribution of each term in the right-hand side of Eq. (25) along the dashed line in Fig. 8 for both the cases with a conducting and an insulating wall, not only J_θ but also the strengths of each of the three terms are quite different between both cases. The main difference between the two cases is seen in the $\mathbf{E} \times \mathbf{b}$ term. That is, the $\mathbf{E} \times \mathbf{b}$ term for the insulating wall is much larger than that of the conducting wall, while the $\mathbf{V} \times \mathbf{B}$ term and the $u_\theta B$ term for the insulating wall are almost the same as the ones for the conducting wall. In other words, the main cause for the reduction of J_θ in the case with a conducting wall is the reduction of the $\mathbf{E} \times \mathbf{b}$ term. This means that when the surface is regarded as a conducting wall, the induced electric field is reduced when compared with the one with an insulating wall. This may be a root cause for the difference of the shock-standoff distance between the insulating wall and the conducting wall.

This reduction of the electric field can be observed in the entire field, as shown in Fig. 11, which depicts the electric potential distribution and the electric current stream lines in the r-z plane around the sphere for the conducting and insulating wall cases. From this figure, we can see that the electric current streamlines and the electric potential distribution for the two cases are quite different. When the surface is the conducting wall, the electric current appears to be short-circuited on the surface. On the other hand, when the surface is the insulating wall, two current loops are created inside the shock layer. While the electric potential difference between the maximum and the minimum values for a conducting wall is about 50 V, the electric potential difference for the insulating wall is about 500 V. The difference of the electric potential distribution between the two cases is significant, and this difference leads to the difference of the electric field strength inside the shock layer. This result suggests that the Hall effect and the surface conductivity have a strong impact on the electric potential distribution inside the shock layer.

From these observations, we can conclude that the electric current, especially the total strength of J_θ, is not affected very much when the vehicle surface is regarded as the insulating wall, even though the Hall effect has a strong impact on the flowfield, such as the electric potential distribution. This is because, as the Hall effect becomes significant, the stronger electric field is generated that, in turn, generates the electric current in the circumferential direction, which is comparable to the one observable in the case of negligible Hall

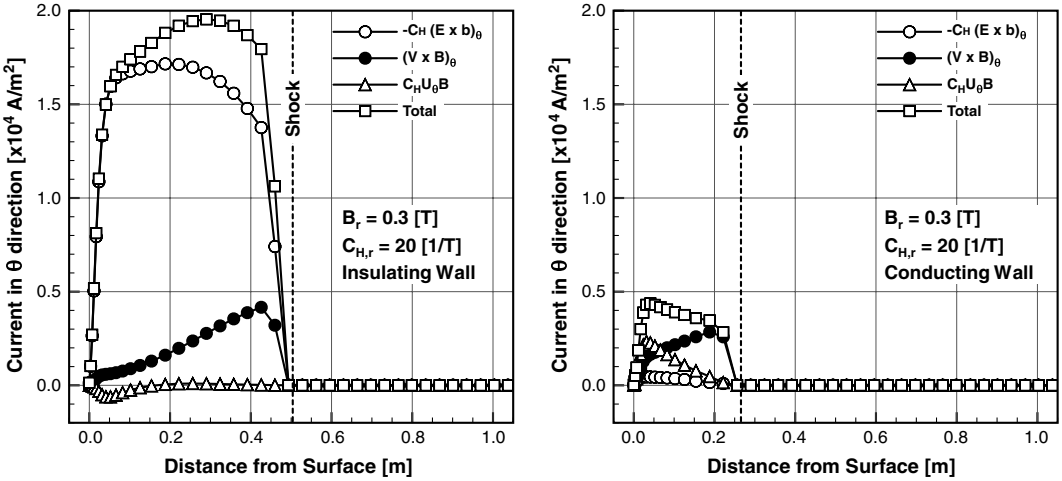

a) Insulating wall b) Conducting wall

Fig. 10 Current strength distribution for the insulating wall and the conducting wall.

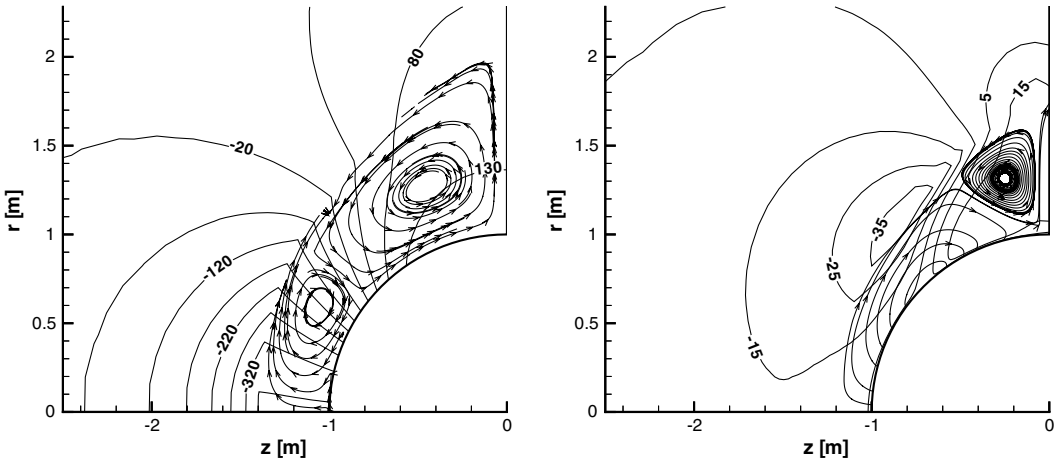

a) Insulating wall b) Conducting wall

Fig. 11 Electric potential distributions and electric current streamlines around the sphere for the insulating wall and the conducting wall.

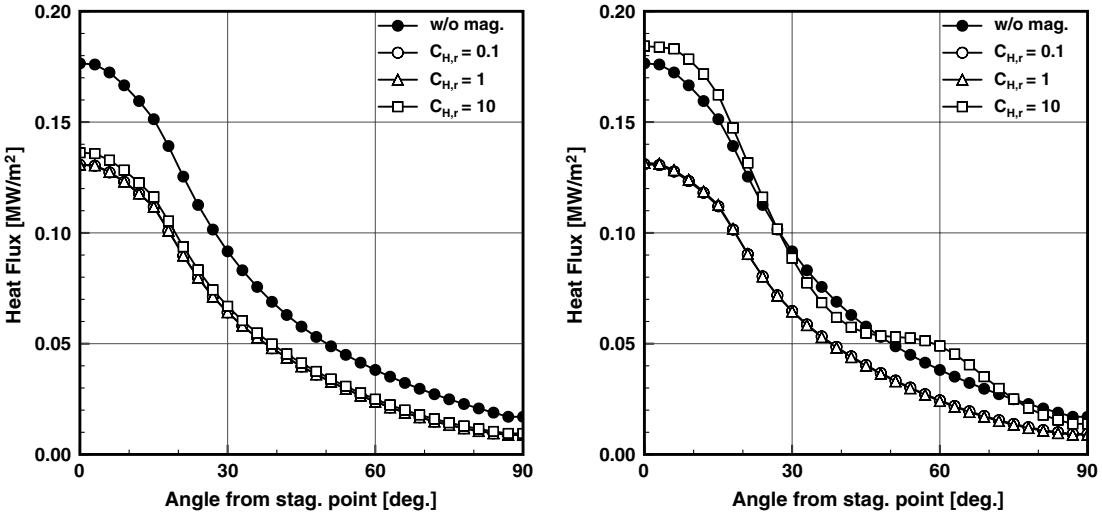

a) Insulating wall b) Conducting wall

Fig. 12 Heat flux distribution along the surface for the insulating wall and the conducting wall.

effect. This is the reason why the shock-standoff distance does not change very much, even when the Hall effect becomes significant. On the other hand, when the vehicle surface is regarded as a conducting surface, the electric field generated through the Hall effect disappears, since it is short-circuited at the vehicle surface and J_θ is never generated. This is the reason why, unlike the nonconducting surface case, the enhancement of the shock-standoff distance almost disappears.

C. Influence of Hall Effect on Heat Flux Mitigation

Figure 12 shows the heat flux distribution along the surface of the sphere, with the conducting and insulating wall condition, with the Hall parameter $C_{H,r}$ of 0.1, 1, and 10. The heat flux distribution without the applied magnetic field is also shown in Figs. 12a and 12b for comparison.

In the case of the insulating wall, the heat flux was reduced by about 30% and, as we can expect from the discussion of the impact of the Hall parameter $C_{H,r}$, on the total strength of J_θ, the efficiency of the EDH was not affected significantly by the Hall effect. This is because the total strength of J_θ and the Lorentz force are not affected significantly by the change of the Hall parameter. From this result, we can confirm that the flight performance of the EDH for the reentry vehicle with the electronically insulating wall is not affected significantly in the wide range of the Hall parameter.

In contrast with the result for the insulating wall, when the surface is the conducting wall, the efficiency is significantly affected by the Hall effect. In the case of a $C_{H,r}$ of 10, the effect of the EDH almost disappears. This is because the total strength of J_θ and the Lorentz force are significantly reduced by the increase of the Hall parameter. This indicates that, in the case of the conducting wall condition, the Hall effect has a negative impact on the efficiency of the EDH.

V. Conclusions

In the present study, we investigated the influence of the Hall effect on the EDH for reentry vehicles by means of a parametric study for the Hall parameter. The simplified flow model was employed in which Navier–Stokes equations with electromagnetic source terms were solved for an ideal gas with electric conductivity.

The present study shows that the Hall effect affects the electric potential distribution and the electric current pattern inside the shock layer drastically, depending on the conductivity of the vehicle surface, but it does not affect, in a wide range of the Hall parameter, including a nominal value, the electric current strength in the circumferential direction in the case of the insulating surface. In the case of the conducting surface, however, the electric current is very much reduced. This phenomenon is caused by the electric potential field in the r-z plane, originating from the Hall effect. The electric current strength in the circumferential direction is a driving force for the shock enhancement phenomenon and is generated by the $\mathbf{V} \times \mathbf{B}$ term in the extended Ohm's law when the Hall effect is neglected. In the case of when the Hall effect is included, however, the electric current is kept in turn by the electric potential field in the case of the insulating surface. In the case of the conducting surface, however, the electric current cannot be kept, since the electric field is short-circuited at the vehicle surface but is significantly reduced. As a result, the shock-standoff distance is not affected very much, even if the Hall effect is significant when the vehicle surface is regarded as an insulating wall. In the case of the conducting surface, however, the shock-standoff distance is reduced, almost down to the value with no magnetic field.

The present parametric study clarified that this behavior is applicable even in a wide range of the Hall parameter and thus suggests that the flight performance of the vehicle equipped with an EDH with an insulating surface is not affected very much, even if the Hall effect varies very much during the flight.

To confirm the above conclusions for the flight performance of the EDH, we investigated the impact of the Hall effect on the heat flux mitigation. In the case of the insulating wall, the heat flux was reduced by about 30%, and the efficiency of the heat flux mitigation is not affected significantly, even if the Hall parameter changes drastically. This is due to the fact that the total strength of J_θ is not affected by the change of the Hall parameter $C_{H,r}$. On the other hand, in the case of the conducting wall, the efficiency was significantly weakened as the Hall parameter increased. From these investigations, we can conclude that the EDH with an electronically insulating surface will be a promising technique for the heat flux mitigation for reentry vehicles.

Acknowledgment

This research was partially supported by the Ministry of Education, Science, Sports, and Culture Grant-in-Aid for Scientific Research (A) (2), 15206093.

References

[1] Poggie, J., and Gaitonde, D. V., "Computational Studies of Magnetic Control in Hypersonic Flow," AIAA Paper 2001-0196, 2001.

[2] Otsu, H., Matsushita, K., Konigorski, D., Funaki, I., and Abe, T., "Reentry Heating Mitigation by Utilizing the Hall Effect," AIAA Paper 2004-2167, 2004.

[3] Levy, R. H., "A Simple MHD Flow with Hall Effect," *AIAA Journal*, Vol. 1, No. 3, 1963, pp. 698–699.
doi:10.2514/3.1617

[4] Porter, R. W., and Cambel, A. B., "Hall Effect in Flight Magnetogasdynamics," *AIAA Journal*, Vol. 5, No. 12, 1967, pp. 2208–2213. doi:10.2514/3.4410

[5] Fujino, T., Sugita, H., Mizuno, M., Funaki, I., and Ishikawa, M., "Influences of Electrical Conductivity of Wall on Magnetohydrodynamic Control of Aerodynamic Heating," *Journal of Spacecraft and Rockets*, Vol. 43, No. 1, 2006, pp. 63–70. doi:10.2514/1.13770

[6] Fujino, T., Matsumoto, Y., Kasahara, J., and Ishikawa, M., "Numerical Studies of Magnetohydrodynamic Flow Control Considering Real Wall Electrical Conductivity," *Journal of Spacecraft and Rockets*, Vol. 44, No. 3, 2007, pp. 625–632. doi:10.2514/1.25824

[7] Wada, Y., and Liou, M.-S., "A Flux Splitting Scheme with High-Resolution and Robustness for Discontinuities," AIAA Paper 1994-0083, 1994.

[8] Shima, E., "Numerical Flow Analysis for HSCT model. (2)," *Special Publication of National Aerospace Laboratory*, No. 41, 1999, pp. 209–214.

[9] Takizawa, Y., Sato, S., Fujita, K., Abe, T., and Konigorski, D., "Electro-Magnetic Effect on a Reentry-Related High-Enthalpy Flow," AIAA Paper 2003-4168, 2003.

K. Powell
Associate Editor